Deep Learning meets Topology-preserving Active Contours: towards scalable quantitative histology of cortical cytoarchitecture.

Konstantin Thierbach[1], Pierre-Louis Bazin[1,2,3], Filippos Gavriilidis[1], Evgeniya Kirilina[1,4], Carsten Jäger[1], Markus Morawski[5], Stefan Geyer[1], Nikolaus Weiskopf[1], and Nico Scherf[1]

[1] Max Planck Institute for Human Cognitive and Brain Sciences, Leipzig, Germany, nscherf@cbs.mpg.de,
[2] Netherlands Institute for Neuroscience, Amsterdam, The Netherlands,
[3] Spinoza Centre for Neuroimaging, Amsterdam, The Netherlands,
[4] Center for Cognitive Neuroscience Berlin, Free University Berlin, Berlin, Germany,
[5] Paul Flechsig Institute of Brain Research, University of Leipzig, Leipzig, Germany

Abstract. Deep learning has thoroughly changed the field of image analysis yielding impressive results whenever enough annotated data can be gathered. While partial annotation can be very fast, manual segmentation of biological structures is tedious and error-prone. Additionally, high-level shape concepts such as topology or boundary smoothness are hard if not impossible to encode in Feedforward Neural Networks. Here we present a modular strategy for the accurate segmentation of neural cell bodies from light-sheet microscopy combining deep learning and topology-preserving geometric deformable models. We show that the network can be trained efficiently from simple cell centroid annotations, and that the final segmentation provides accurate detection and smooth segmentations, without introducing cell splitting or merging.

Keywords: histology, image segmentation, cell detection, deep learning, convolutional neural networks, active contours

1 Introduction

Systematic studies of the cortical cytoarchitecture are indispensable to understand the functional organization of the human brain. Classical works based on qualitative description of cell counts and shapes in physical 2D sections of the human cortex revealed functional areas in the brain[3, 6, 17]. These brain parcellations are currently updated and refined using automated image analysis [21]. Even 3D imaging of post mortem brain tissue at microstructural resolution are within reach using recent light sheet fluorescence microscopy (LSFM) [9, 5] and tissue clearing protocols [4]. Combined with advanced image analysis these techniques open the door for studying cortical cellular organisation in the human brain with unsurpassed precision. Such studies are crucial to validate in

vivo MRI-based cortical architecture mapping[18] to understand the relationship between structure and function in the human brain. To reach this goal we need reliable computational analysis with minimal manual annotations, facing the following challenges:

- Clearing of aged, unperfused human tissue is imperfect and optical distortions due to scattering and refraction remain. This leads to varying background intensities across the image and shadow artifacts.
- The penetration of antibody stains is uneven across the sample. The tissue degenerates with longer post-mortem times. These effects increase the already high variability of neural shape and appearance in the cortical samples.
- Cell density varies locally, leading to false segmentation of cells into clusters.

Machine Learning methods improved the analysis of microscopy data [16, 1, 8]. Deep Learning, in particular Convolutional Neural Networks (CNNs), can address challenging problems in biomedical imaging because they learn multi-level internal representations of the data [12, 15]. These, typically supervised, methods require a lot of annotated data: For cell segmentation pixel-accurate masks have to be supplied [14]. Manually annotating data for training is often prohibitive in biomedical applications where data are specialized, scarce and expert knowledge is required. Abstract concepts at the object level (Gestalt principles such as continuation, closure [10], or object topology) are hard to learn with CNNs. Additional annotation of the border region between adjacent cells is needed to reduce false merging of neighboring cells [14]. Human vision exploits high level concepts using top-down processing [10] which is not represented in feedforward architectures.

Active Contour methods have been designed to embody high level concepts of object shapes. They can guarantee the smoothness of contours and a consistent topology [2, 7]: features that improve cell segmentation in challenging conditions and prevents splitting and merging of contours during segmentation. But active contour methods require an initialization with the number and approximate position of objects in the image. Robust initial localization of cells is hard to define a priori and should be learned from data. This is where Deep Learning has a clear advantage: Convolutional neural networks can be trained to robustly predict cell positions in images using only sparse centroid annotations [19].

In this work we combine the complementary strengths of CNNs and topology-aware active contours into a robust workflow to detect and segment cells that delivers high quality results and requires only minimal annotations (sparse annotations of approximate cell centers are enough)[6]. Here, we demonstrate the feasibility of this idea in a proof of concept study using 2D slices from a 3D microscopy image volume obtained of cleared post mortem human brain blocks, but the required methods can be extended to 3D as well.

[6] A related approach combining deep learning and active contours has been proposed by[11] to segment vertebral bodies in MR spine images.

2 Methodology

2.1 Sample Preparation

Blocks from a human post mortem brain (temporal lobe cortex, male, 54 yr., post-mortem interval 96h) have been provided by the Brain Banking Centre Leipzig of the German Brain-Net. The entire procedure of case recruitment, acquisition of the patient's personal data, the protocols and the informed consent forms, performing the autopsy, and handling the autoptic material have been approved by the local ethics committee. For details on tissue preparation and clearing see [13].

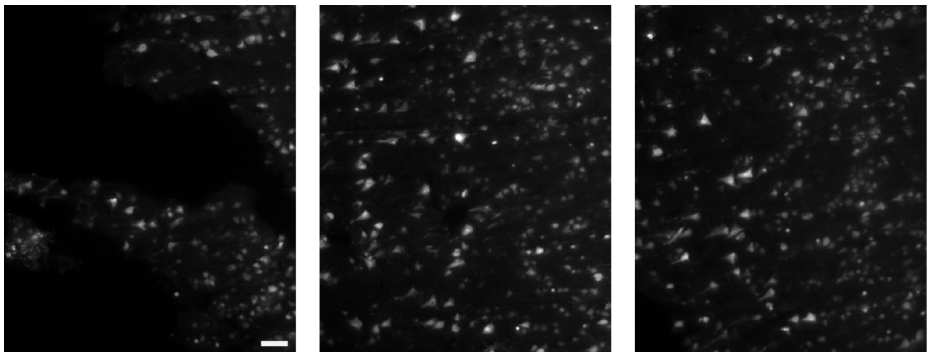

Fig. 1. Image data. Three samples images from the stack at different imaging depths (left to right: 0mm, 1mm, 2mm; scale bar 100 μm).

2.2 Image Data

A commercial light-sheet fluorescence microscope (LaVision BioTec, Bielefeld, Germany) was used to image the cleared specimen. The microscope was equipped with 10x CLARITY-objective (Olympus XLPLN10XSVMP, numerical aperture (NA) 0.6, working distance (WD) 8 mm; Zeiss Clr Plan-Apochromat, NA 0.5, WD 3.7 mm) and operated with 630 nm excitation wavelength and band-pass 680 nm emission filter. Samples were stained with a fluorescent monoclonal antibody against human neuronal protein HuC/HuD (a specific marker for neuronal cells). The acquisition covered a 1.1 mm x 1.3 mm x 2.5 mm volume resulting in a stack of 2601 16 bit TIFF images (2560 x 2160 pixels, 0.51 μm lateral resolution) using a 1 μm step size.

For the 2D analysis workflow we took 19 slices at regular intervals from the entire stack. We used 15 images for training and validation and kept 4 images as a test set. The images for the test set were used for final assessment of segmentation performance only. A single image typically contains around 300 cells (Fig. 1).

2.3 Cell Segmentation Workflow

Our modular approach is based on version A of the Fully Convolutional Regression Network architecture (FCRN-A)[19] to robustly predict cell positions and a topology-preserving multi-contour segmentation [2] to control smoothness and topology of the segmentation. The basic concept of our approach (Fig. 2) is as follows:

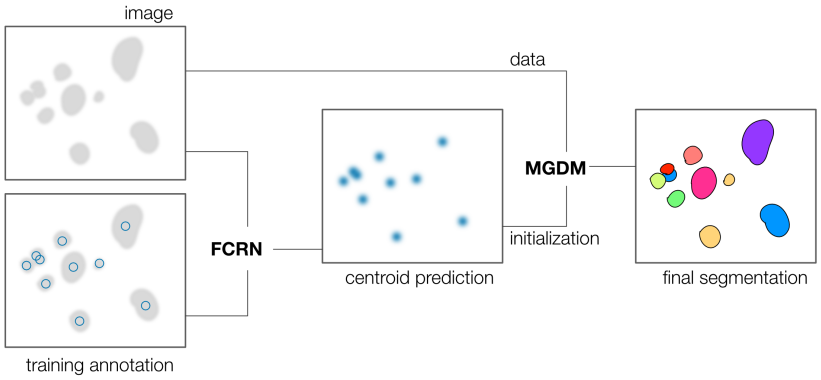

Fig. 2. Schematic overview of method. We train a FCRN network on manually labeled cell centroids. The predicted cell positions are used as initialization and topology prior for the multi-object contour segmentation.

- **Training step:** Pairs of images (annotated centroids and raw data) are fed into FCRN. The network is trained to predict a Gaussian distribution around the expected cell centroid.
- **Prediction step:** FCRN predicts probability maps of cell positions from the raw image. These centroid probabilities are filtered for local maxima to initialize the active contour segmentation that segments the cells from the raw images.

Cell Detection We adapted the FCRN-A architecture from [19]. We trained the network on randomly sampled image sections of size 512x512 pixels and the annotated centroids. We discarded sections which did not contain any annotated cells to improve convergence. Further, we applied data augmentation to the training samples in form of image rotation up to 90° and image translations in x and y direction of up to 20% of the image size. For optimization we used stochastic gradient descent with a batch size of 32, and an adaptive learning rate (ADADELTA) [20].

Multi-object Geometric Deformable Model Once cell centroids have been detected, the final segmentation is handled by a Multi-object Geometric Deformable Model (MGDM) which ensures fast segmentation of an arbitrarily large number of cells while enforcing topological constraints [2]. The deformable model is driven by curvature regularization and balloon forces derived from the microscopy image intensities as follows.

For each detected cell, we first find the maximum intensity M_c inside the initial centroid probability map. We set the balloon forces to decrease linearly with the distance to M_c:

$$F_c(x) = \frac{M_c - |I(x) - M_c|}{M_c}. \tag{1}$$

where $I(x)$ is the image intensity. Because fluorescence intensity varies between cells, this calibration ensures that each cell is within its detection range. For the background, we first estimate the mean image intensity M_B to separate background from cells and derive a similar balloon force:

$$F_B(x) = \frac{2M_B - I(x)}{M_B} \tag{2}$$

To avoid unstable evolution from too large forces, F_c and F_B are all bounded in $[+1, -1]$. Balloon and curvature forces are combined in the MGDM evolution equation:

$$\frac{\partial \phi_{c,B}}{\partial t} = (w_\kappa \kappa + w_{c,B} F_{c,B}) |\nabla \phi_{c,B}| \tag{3}$$

For this study we fixed the weights for curvature regularization to $w_\kappa = 0.6$, and the balloon forces to $w_{c,B} = 0.3$. The evolution was run for 200 iterations.

Validation of Results An expert created reference cell masks on the test images. The masks were independently checked and corrected by a second expert. To assess cell detection accuracy, we computed precision $p = \frac{TP}{TP+FP}$, recall $r = \frac{TP}{TP+FN}$, and the combined F-score=$2\frac{p*r}{p+r}$; TP are true positive, FP false positive, and FN false negative detections. Since false splitting and fusion of cell masks are not explicit in these measures, we report those rates separately as the ratio of splits and fusions to the total number of reference cells. To validate the agreement between annotated masks and segmentation we computed the Jaccard index between each reference cell mask A and the best-fitting mask B of the result: $J(A, B) = \frac{|A \cap B|}{|A| + |B| - |A \cap B|}$.

We used the fastER segmentation [8] as a reference baseline because it produces state-of-the art results on par with deep learning methods such as [14] and can be trained with few annotations[7].

[7] Note that fastER is limited to 2D images only.

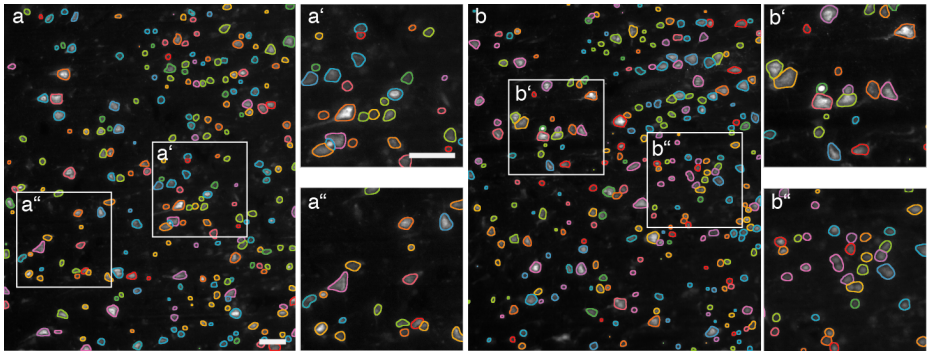

Fig. 3. Segmentation result. Two images from the test set showing outlines of segmented cell masks, subregions were magnified for better visibility (scale bar 100 μm).

3 Results

Examples of final segmentation masks on the test set are shown in Fig.3. The segmentation performed well across regions with varying cell appearance and density. The cell localization step produced a few fusion and splitting errors, particularly in regions where small, dim cells were concentrated (Fig.3 b").

Quantitative results were aggregated over all four test images and summarized in Table 3. The proposed method improved cell detection and particularly segmentation accuracy. For a more detailed picture the distribution of the Jaccard index over all 992 masks is shown in Fig. 3a.

method	precision	recall	F-score	merge rate	split rate	JI(median)
ours	**0.891**	**0.943**	**0.917**	0.011	**0.002**	**0.713**
FastER	0.834	0.917	0.874	**0.007**	0.007	0.521

Table 1. Comparison of segmentation across test set. Best results shown in bold.

As we were interested in how segmentation impacts downstream analysis, we compared the estimated cell size distribution[8] in Fig. 3b. While our results slightly overestimate cell sizes, the distribution was much closer to the reference data than fastER.

4 Conclusions

As a proof of concept we present a modular strategy to segment neural cells combining deep learning and a topology-preserving geometric deformable model. Our method improves cell detection and robustly segments cell bodies in light-sheet

[8] Cell size is an important feature to classify cell types and define cortical layers.

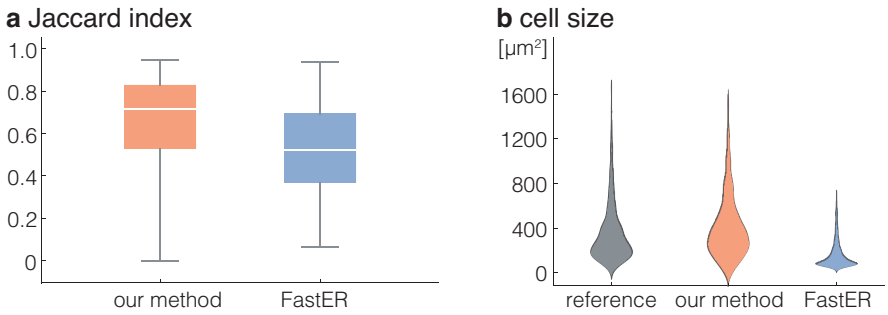

Fig. 4. Quantitative comparison of segmentation. Distribution of (a) segmentation accuracy across test set and (b) extracted cell sizes against reference.

microscopy images of cleared post mortem human brain tissue. Good results were obtained despite varying background and cell intensities. Our method only requires sparse annotation for training and can be easily adapted to improved clearing, staining and imaging protocols. Most importantly, the methods can be extended to the full 3D image data, where the advantage of using only sparse annotations is crucial for large-scale histological analysis of desired quality.

As a next step we will concentrate on further optimizing the regression network to better handle differences in cell appearance and to further improve detection.

Our results highlight a general point: Classical approaches based on mathematical models and Machine Learning are often complementary and a combined strategy can benefit from learning sensitive parts directly from data (e.g. initialization, features) while exploiting the high-level information supplied by the model.

References

1. Arganda-Carreras, I., Kaynig, V., Rueden, C., Eliceiri, K.W., Schindelin, J., Cardona, A., Sebastian Seung, H.: Trainable weka segmentation: a machine learning tool for microscopy pixel classification. Bioinformatics 33(15), 2424–2426 (2017)
2. Bogovic, J.A., Prince, J.L., Bazin, P.L.: A multiple object geometric deformable model for image segmentation. Comput. Vis. Image Underst. 117(2), 145–157 (2013)
3. Brodmann, K.: Vergleichende Lokalisationslehre der Grosshirnrinde in ihren Prinzipien dargestellt auf Grund des Zellenbaues. Barth (1909)
4. Chung, K., Deisseroth, K.: CLARITY for mapping the nervous system. Nat. Methods 10(6), 508–513 (2013)
5. Dodt, H.U., Leischner, U., Schierloh, A., Jährling, N., Mauch, C.P., Deininger, K., Deussing, J.M., Eder, M., Zieglgänsberger, W., Becker, K.: Ultramicroscopy: three-dimensional visualization of neuronal networks in the whole mouse brain. Nat. Methods 4(4), 331–336 (2007)

6. von Economo, C.F., Koskinas, G.N.: Die cytoarchitektonik der hirnrinde des erwachsenen menschen. J. Springer (1925)
7. Han, X., Xu, C., Prince, J.L.: A topology preserving level set method for geometric deformable models. IEEE Transactions on Pattern Analysis and Machine Intelligence 25(6), 755–768 (2003)
8. Hilsenbeck, O., Schwarzfischer, M., Loeffler, D., Dimopoulos, S., Hastreiter, S., Marr, C., Theis, F.J., Schroeder, T.: fastER: a user-friendly tool for ultrafast and robust cell segmentation in large-scale microscopy. Bioinformatics (2017)
9. Huisken, J., Swoger, J., Del Bene, F., Wittbrodt, J., Stelzer, E.H.K.: Optical sectioning deep inside live embryos by selective plane illumination microscopy. Science 305(5686), 1007–1009 (2004)
10. Kandel, E.R., Schwartz, J.H., Jessell, T.M., Siegelbaum, S.A., Hudspeth, A.J., Others: Principles of neural science, vol. 4. McGraw-hill New York (2000)
11. Korez, R., Likar, B., Pernuš, F., Vrtovec, T.: Model-Based segmentation of vertebral bodies from MR images with 3D CNNs. In: Medical Image Computing and Computer-Assisted Intervention – MICCAI 2016. pp. 433–441. Lecture Notes in Computer Science, Springer, Cham (2016)
12. LeCun, Y., Bengio, Y., Hinton, G.: Deep learning. Nature 521(7553), 436–444 (2015)
13. Morawski, M., Kirilina, E., Scherf, N., Jäger, C., Reimann, K., Trampel, R., Gavriilidis, F., Geyer, S., Biedermann, B., Arendt, T., Weiskopf, N.: Developing 3D microscopy with CLARITY on human brain tissue: Towards a tool for informing and validating MRI-based histology. Neuroimage (Nov 2017)
14. Ronneberger, O., Fischer, P., Brox, T.: U-Net: Convolutional networks for biomedical image segmentation. In: Navab, N., Hornegger, J., Wells, W.M., Frangi, A.F. (eds.) Medical Image Computing and Computer-Assisted Intervention – MICCAI 2015. pp. 234–241. Lecture Notes in Computer Science, Springer International Publishing (2015)
15. Shen, D., Wu, G., Suk, H.I.: Deep learning in medical image analysis. Annu. Rev. Biomed. Eng. (2017)
16. Sommer, C., Straehle, C., Köthe, U., Hamprecht, F.A.: Ilastik: Interactive learning and segmentation toolkit. In: 2011 IEEE International Symposium on Biomedical Imaging: From Nano to Macro. pp. 230–233 (2011)
17. Vogt, C., Vogt, O.: Allgemeine ergebnisse unserer hirnforschung I–IV. J. Psychol. Neurol. (Lpz.) 25, Erg. heft 1, 279–462 (1919)
18. Weiskopf, N., Mohammadi, S., Lutti, A., Callaghan, M.F.: Advances in MRI-based computational neuroanatomy: from morphometry to in-vivo histology. Curr. Opin. Neurol. 28(4), 313–322 (2015)
19. Xie, W., Noble, J.A., Zisserman, A.: Microscopy cell counting and detection with fully convolutional regression networks. Computer Methods in Biomechanics and Biomedical Engineering: Imaging and Visualization pp. 1–10 (2016)
20. Zeiler, M.D.: Adadelta: An adaptive learning rate method. CoRR abs/1212.5701 (2012)
21. Zilles, K., Schleicher, A., Palomero-Gallagher, N., Amunts, K.: Quantitative analysis of cyto-and receptor architecture of the human brain. In: Brain Mapping: The Methods (Second Edition), pp. 573–602. Elsevier (2002)